NASA Contractor Report 189176

Low Re Multiple-Time-Scale Turbulence Model and Calculations of Steady and Pulsating Shear Layers

Sang-Wook Kim
University of Toledo
Toledo, Ohio

May 1992

Prepared for
Lewis Research Center
Under Cooperative Agreement NCC3–229

National Aeronautics and
Space Administration

Low Re multiple-time-scale turbulence model and calculations of steady and pulsating shear layers

Sang-Wook Kim*
University of Toledo
Toledo, Ohio 43606

ABSTRACT

A low Reynolds number multiple-time-scale turbulence model (LMS) and its application to fully developed turbulent channel flows and pulsating pipe flows are presented. The LMS can describe the inequilibrium turbulence phenomena down to the viscous sublayer. The calculated fluid flow and turbulence fields for the channel flows are in better agreement with the direct numerical simulation (DNS) results than those obtained using a Reynolds stress turbulence model, and the calculated near-wall dissipation rates are in qualitatively correct agreement with the DNS results. The LMS also successfully predicts the rapidly varying phase-lead of the wall shearing stress that occurs in a narrow range of the dimensionless frequency ($\omega^+ = \omega\nu/u_\tau^2$) for the pulsating pipe flows while various other turbulence models fail to predict this phenomenon, and the LMS yields significantly improved numerical results for a wide range of the dimensionless frequency compared with those obtained using a rapid distortion theory (RDT).

---

*NASA Resident Research Associate at Lewis Research Center.

NOMENCLATURE

c_{pi}	model constants for ε_p equation (i=1,3)
c_{ti}	model constants for ε_t equation (i=1,3)
c_μ	eddy viscosity coefficient
$c_{\mu f}$	constant coefficient (=0.09)
f	frequency
f_μ	wall damping function for eddy viscosity equation
k	turbulent kinetic energy ($k=k_p+k_t$)
k^+	normalized turbulent kinetic energy ($=k/u_\tau^2$)
k_p	turbulent kinetic energy in production range
k_p^+	normalized k_p ($=k_p/u_\tau^2$)
k_t	turbulent kinetic energy in dissipation range
k_t^+	normalized k_t ($=k_t/u_\tau^2$)
p	pressure
P_r	production rate
Re	Reynolds number
R_y	turbulent Reynolds number ($=\sqrt{k}y/\nu$)
T	period of oscillation
u_b	bulk velocity
u	time averaged velocity
u^+	non-dimensional velocity ($=u/u_\tau$)
u_τ	friction velocity ($=\sqrt{\tau_w/\rho}$)
$\overline{u'v'}$	Reynolds stress
$\overline{u'v'}^+$	normalized Reynolds stress ($=\overline{u'v'}/u_\tau^2$)
x_j	spatial coordinates ($=\{x,y,z\}$)
y^+	wall coordinate ($=yu_\tau/\nu$)
δ_s	Stokes layer thickness ($=\sqrt{2\nu/\omega}$)
ε_p	energy transfer rate

ε_p^+ nomalized energy transfer rate ($=\nu\varepsilon_p/u_\tau^4$)

ε_t dissipation rate

ε_t^+ nomalized dissipation rate ($=\nu\varepsilon_t/u_\tau^4$)

μ molecular viscosity

ν kinematic viscosity

τ_w wall shearing stress

μ_t turbulent viscosity

ρ density

σ_i turbulent Prandtl number for i-equation, $i=\{k_p,\varepsilon_p,k_t,\varepsilon_t\}$

ω angular velocity ($=2\pi f$)

ω^+ dimensionless frequency ($=\omega\nu/u_\tau^2$)

Superscripts

$'$ fluctuating velocity component

$\overline{()}$ time-averaged value

$\widetilde{()}$ ensemble-averaged value

$|\widetilde{()}|$ amplitude of oscillation

Subscripts

j denotes spatial coordinates ($=\{x,y,z\}$)

1. Introduction

Either the development of a new near-wall turbulence model or the improvement of various near-wall turbulence models are hindered due to the lack of detailed knowledge on the near-wall turbulence structure especially that for the near-wall dissipation rate. Recently, Kim et al. (1987) provided detailed near-wall turbulence data for fully developed channel flows obtained from direct numerical simulations. The validity of the DNS results is established by comparing them with measurable turbulence quantity. A near-wall dissipation rate obtained from the DNS results and that proposed by Patel et al. (1985) are shown in figure 1. The dissipation rate obtained from the DNS results show that the peak value is located at the wall while the dissipation rate model proposed by Patel et al. (1985) shows that the dissipation rate attains its peak value at $y^+ \sim 12$. Numerical calculations using various turbulence models yield near-wall dissipation rates similar to the one proposed by Patel et al. (1985). It is not clear if there exist any turbulence model that can yield a near-wall dissipation rate that is in qualitatively correct agreement with the DNS result and that can also yield accurate numerical results for a few different classes of turbulent flows. Consequently, the influence that the two distinctly different near-wall dissipation rates can cause on numerical calculations of turbulent flows is not known yet. The discrepancy that can be caused by the different near-wall dissipation rates are discussed in this paper.

Numerous efforts have been made to develop or to improve turbulence models to correctly predict steady simple shear layers as well as complex turbulent flows. However, only a very small amount of efforts has been made for numerical investigations of unsteady turbulent flows. Calculations

of a pulsating pipe flow using an algebraic turbulence model, a k-ε turbulence model, and a Reynolds stress turbulence model (RSM) can be found in Kebede et al. (1985). It can be seen in the reference that the algebraic turbulence model yields the most accurate numerical results and the RSM yields the worst numerical results, and the cause for the deteriorated numerical results obtained using the RSM is not clearly known. Mao & Hanrathy (1986) carried out experimental and numerical investigations of pulsating pipe flows. Calculations of the pulsating pipe flows at a wide range of the dimensionless frequency (ω^+) revealed that an algebraic turbulence model discussed in the Thorseness et al. (Mao & Hanrathy, 1986) yields qualitatively inaccurate numerical results while a pressure-relaxation algebraic turbulence model yields numerical results that are in good agreement with the measured data. However, it is admitted in Mao & Hanrathy (1986) that the pressure-relaxation model lacks a theoretical background. More recently, Mankbadi & Liu (1992) developed an algebraic turbulence model based on the rapid distortion theory (RDT) and showed that the turbulence model yields accurate numerical results for pulsating pipe flows at high dimensionless frequency while the turbulence model still can not yield accurate numerical results for the flows at low dimensionless frequency. As is obvious from the above discussion, numerical investigations of unsteady turbulent flows are mostly made using algebraic turbulence models since k-ε or RSM does not yield accurate numerical results. However, applicability of algebraic turbulence models is limited since these turbulence models can not yield accurate numerical results for various complex turbulent flows.

The multiple-time-scale turbulence model presented in this paper is based on a simplified split-spectrum method (Hanjelic et al. 1980; Kim &

Chen 1989). In the high Reynolds number multiple-time-scale turbulence model presented in Kim & Chen (1989), the near-wall turbulence field is described using a wall function method. This turbulence model yields accurate numerical results for complex turbulent flows in case the turbulence field is not strongly influence by the near-wall turbulence structure. Such turbulent flow cases can be found in a turbulent flow over a backward-facing step, a wall-jet flow, and confined coaxial jets with and without swirling velocity components. Later, the predictive capability of the turbulence model was improved by incorporating a "partially low Reynolds number near-wall turbulence model" into the multiple-time-scale turbulence equations (PLMS). In the PLMS (Kim 1990, 1991; Kim & Benson 1992), the near-wall turbulence field is described by a single time-scale turbulence model derived from a k-equation turbulence model. The PLMS yields significantly improved numerical results for the turbulence structure in the near-wall region. It can be found in Kim (1990) that the PLMS successfully predicts the extensive growth of the shock-separated recirculation region in the transonic flow over a curved hill. It can also be found in Kim & Benson (1992) that the PLMS can accurately resolve the strong interaction between circular jets and crossflows and successfully predicts the horse-shoe vortex located along the circumferences of the jet exits. Unfortunately, the turbulence model still can not yield accurate numerical results for a class of turbulent flows in which the entire fluid flow is strongly governed by the near-wall turbulence structure since, in such cases, a large portion of the turbulence field is described by a single time-scale k-equation turbulence model. This class of turbulent flows can be found in fully developed channel flows at very low Reynolds numbers and unsteady pulsating pipe flows. In this paper, a new improvement is

incorporated into the multiple-time-scale turbulence model to accurately resolve this class of turbulent flows and to extend the applicability of the turbulence model to wider classes of turbulent flows..

The time averaged or the ensemble averaged Navier-Stokes equations and the turbulence equations are solved by a finite volume method that incorporates a pressure-staggered mesh and a partial differential equation for incremental pressure (Kim 1990, 1991; Kim & Benson 1991, 1992). Various laminar and turbulent flows solved using the numerical method include: reattaching shear layers in a divergent channel, transonic turbulent flows with shock wave - boundary layer interaction, three-dimensional turbulent flows of circular jets in crossflows, and self-sustained unsteady flows over a circular cylinder and a square cylinder. Details of the numerical method and the independence tests of the numerical method on the grid size and on the time-step size can be found in Kim & Benson (1991) and the references cited therein. It can also be found in these references that the present numerical method yields accurate numerical results for separated and recirculating flows using highly graded meshes.

2. Low Re multiple-time-scale turbulence equations

In the multiple-time-scale turbulence models, the turbulent transport of mass and momentum is described using the time-scale of large eddies and the dissipation rate is described using the time-scale of fine-scale eddies (Kim & Chen 1989; Kim & Benson 1992). In this regard, the convection-diffusion equations of the multiple-time-scale turbulence models describe the physically observed turbulence phenomena most naturally. The use of multiple time-scales also enables the turbulence equations to resolve the

"inequilibrium turbulence" phenomena and to model the cascade process of the turbulent kinetic energy. Here, the "inequilibrium turbulence" represents the state of a turbulence field in which P_T/ε_t varies rapidly in space so that the shape and the frequency domain of the spectral density varies widely in space. The influence of the inequilibrium turbulence on turbulent transport of mass and momentum can be observed in a number of semi-emperical data (theoretically derived data from a set of measured data). Detailed analyses of these capabilities can be found in Kim & Benson (1992) and the pertinent results are presented in the "Inherent capability of LMS equations" sub-section.

It can be seen in Kim & Benson (1992) and the references cited therein that the numerical results for various complex turbulent flows (e.g., turbulent flows subjected to extra strains caused by streamline curvature, interaction of multiple number of shear layers, and shock wave-boundary layer interactions) obtained using the multiple-time-scale turbulence model are in as good agreement with the measured data as those obtained using an optimized k-ε turbulence model, algebraic Reynolds stress turbulence model (ARSM) or RSM for each flow. Undoubtedly, the anisotropy of the turbulence is the most easily detectable phenomenon in a measurement of a turbulent flow and hence, in theoretical investigations of turbulence, the emphasis was laid upon improving the ARSM and the RSM. However, numerous numerical investigations carried out during the last decades show that the ARSM and RSM still can not accurately predict the turbulence phenomena occurring in various flows unless the pressure-strain rate correlation is optimized for each flow. The capability of the multiple-time-scale turbulence model to solve widely different complex turbulent flows is attributed to its capability to resolve the inequilibrium

turbulence and to model the cascade of the turbulent kinetic energy. A low Reynolds number multiple-time-scale turbulence model that can resolve the inequilibrium turbulence phenomena down to the viscous sublayer and calculations of turbulent flows that are highly sensitive to the near-wall turbulence structure are presented in this paper.

2.1. *LMS equations*

The multiple-time-scale turbulence equations that include the near-wall modifications are described below. The turbulent kinetic energy (k_p) and the energy transfer rate (ε_p) equations for energy containing large eddies are given as;

$$\frac{\partial}{\partial t}(\rho k_p) + \frac{\partial}{\partial x_j}(\rho u_j k_p) - \frac{\partial}{\partial x_j}\left\{\left(\mu + \frac{\mu_t}{\sigma_{kp}}\right)\frac{\partial k_p}{\partial x_j}\right\} = \rho P_r - \rho \varepsilon_p \tag{1}$$

$$\frac{\partial}{\partial t}(\rho \varepsilon_p) + \frac{\partial}{\partial x_j}(\rho u_j \varepsilon_p) - \frac{\partial}{\partial x_j}\left\{\left(\mu + \frac{\mu_t}{\sigma_{\varepsilon p}}\right)\frac{\partial \varepsilon_p}{\partial x_j}\right\} = \frac{\rho}{k_p}(c_{p1}P_r^2 + c_{p2}P_r\varepsilon_p - c_{p3}f_{\varepsilon p}\varepsilon_p^2) \tag{2}$$

where ρ is the density, u_j ($=\{u,v\}$) is the ensemble-averaged velocity, μ is the molecular viscosity, μ_t is the turbulent viscosity, σ_{kp} and $\sigma_{\varepsilon p}$ are the turbulent Prandtl numbers for the k_p- and ε_p-equation, respectively, c_{pi} ($i=1,3$) are model constants, and the production rate (P_r) is given as

$$P_r = \frac{\mu_t}{\rho}\left\{2\left(\frac{\partial u}{\partial x}\right)^2 + 2\left(\frac{\partial v}{\partial y}\right)^2 + \left(\frac{\partial u}{\partial y} + \frac{\partial v}{\partial x}\right)^2\right\}$$

The turbulent kinetic energy (k_t) and the dissipation rate (ε_t) equations for fine scale eddies are given as:

$$\frac{\partial}{\partial t}(\rho k_t) + \frac{\partial}{\partial x_j}(\rho u_j k_t) - \frac{\partial}{\partial x_j}\left\{\left(\mu + \frac{\mu_t}{\sigma_{kt}}\right)\frac{\partial k_t}{\partial x_j}\right\} = \rho \varepsilon_p - \rho \varepsilon_t \tag{3}$$

$$\frac{\partial}{\partial t}(\rho\varepsilon_t) + \frac{\partial}{\partial x_j}(\rho u_j \varepsilon_t) - \frac{\partial}{\partial x_j}\left[\left(\mu + \frac{\mu_t}{\sigma_{\varepsilon t}}\right)\frac{\partial \varepsilon_t}{\partial x_j}\right] = \frac{\rho}{k_t}(c_{t1}\varepsilon_p^2 + c_{t2}\varepsilon_p\varepsilon_t - c_{t3}f_{\varepsilon t}\varepsilon_t^2) \qquad (4)$$

where σ_{kt} and $\sigma_{\varepsilon t}$ are the turbulent Prandtl numbers for the k_t- and ε_t-equation, respectively, and c_{ti} (i=1,3) are model constants. The turbulent eddy viscosity is given as;

$$\mu_t = \rho c_{\mu f} f_\mu \frac{k^2}{\varepsilon_p} \qquad (5)$$

The turbulence model constants for the LMS equations are given as; $c_{pi}(i=1,3) = \{0.21, 1.32, 1.84\}$, $c_{ti}(i=1,3) = \{0.32, 1.21, 1.65\}$, $\sigma_{kp} = \sigma_{kt} = 0.75$, $\sigma_{\varepsilon p} = \sigma_{\varepsilon t} = 1.15$, and $c_{\mu f} = 0.09$. A few model constants in c_{pi} and c_{ti} are slightly different from those used in the PLMS. Calculations of free shear layers and complex turbulent flows using the LMS show that the inequilibrium turbulence structure in the external region is not influenced significantly by the slightly re-distributed model constants. Furthermore, many complex turbulent flows are not strongly influenced by the near-wall turbulence structure so that the numerical results for complex turbulent flows obtained using the LMS are only slightly better than or almost the same as those obtained using the PLMS.

The high Reynolds number ε_p- and ε_t-eauation can not correctly describe the inequilibrium turbulence phenomena in the near-wall region since the wall proximity and the molecular viscosity dominate the development of the turbulence field in the region. The wall damping functions $f_{\varepsilon p}$ and $f_{\varepsilon t}$ are constructed in such a way that the functions reproduce physically consistent near-wall distributions of ε_p and ε_t and render the partial differential equations well posed at y~0. The wall

damping functions f_μ, $f_{\varepsilon p}$ and $f_{\varepsilon t}$ are described later in the "Near-wall turbulence" sub-section.

2.2. *Near-wall ε_p and ε_t*

The near-wall ε_p and ε_t are obtained from analytical solutions of the k_p- and k_t- equation. Adding up equations (1) and (3) yields

$$\frac{\partial}{\partial t}(\rho k) + \frac{\partial}{\partial x_j}(\rho u_j k) - \frac{\partial}{\partial x_j}\left\{\left(\mu + \frac{\mu_t}{\sigma_k}\right)\frac{\partial k}{\partial x_j}\right\} = \rho P_r - \rho\varepsilon_t \qquad (6)$$

where k ($=k_p+k_t$) is the turbulent kinetic energy. At very close to the wall (y~0), the molecular diffusion term and the dissipation rate dominate over the other terms in equation (6) since k≈0, Pr≈0 and μ_t≈0. Formally integrating $-\partial\{\mu(\partial k/\partial x_j)\}/\partial x_j = -\rho\varepsilon_t$ yields

$$\varepsilon_t = 2\nu k/y^2 \qquad (7)$$

where $\nu=\mu/\rho$ is the kinematic viscosity. The dissipation rate obtained using equation (7) and the turbulent kinetic energy of DNS results for $Re(u_\tau)$ = 180 are compared with that of DNS result in figure 1, where u_τ ($=\sqrt{\tau_w/\rho}$) is the friction velocity and τ_w is the wall shearing stress. The near-wall dissipation rate obtained using $\varepsilon_t = 2\nu(\partial\sqrt{k}/\partial y)^2$ is also shown in the figure. The latter expression is used in a number of low Reynolds number turbulence models cited in Patel et al. (1985) and in the RSM proposed by Lai & So (1990). It can be seen in the figure that the near-wall dissipation rate obtained using equation (7) compares more favorably with the DNS result for a wider range of y^+ than that obtained using $\varepsilon_t = 2\nu(\partial\sqrt{k}/\partial y)^2$, where $y^+=yu_\tau/\nu$ is the normalized distance from the wall. It can also be seen in the figure that the slope of the dissipation rate obtained using

equation (7) is less steeper than that of the DNS result. The less steeper slope is caused by neglecting the turbulent diffusion term in deriving equation (7). Similarly, the energy transfer rate for y~0 is obtained by formally integrating equation (2) and is given as

$$\varepsilon_p = 2\nu k_p / y^2 \tag{8}$$

In the present calculations, the near-wall ε_p and ε_t for $R_y<5$ (which corresponds to $y^+<2\sim3$) are obtained using equations (7) and (8), where $R_y = \sqrt{k}\,y/\nu$ is the turbulent Reynolds number based on the distance from the wall.

2.3. *Near-wall turbulence*

The instantaneous velocities in the viscous sublayer can be written as (Patel et al. 1985)

$$\left.\begin{aligned} u' &= a_1 y + a_2 y^2 + \ldots\ldots \\ v' &= \quad\; b_2 y^2 + \ldots\ldots \\ w' &= c_1 y + c_2 y^2 + \ldots\ldots \end{aligned}\right\} \tag{9}$$

where a_i, b_i, and c_i are functions of time, $\overline{a_i} = \overline{b_i} = \overline{c_i} = 0$, and the over-bar denotes a time-averaged value. The fluctuating normal velocity grows in proportion to the square of the distance from the wall due to the wall proximity. Thus the turbulent kinetic energy and the Reynolds stress in the region very close to the wall (y~0) can be written as;

$$\left.\begin{aligned} k &= \frac{1}{2}\left(\overline{u'^2} + \overline{v'^2} + \overline{w'^2}\right) = \frac{1}{2}\left(\overline{a_1^2} + \overline{c_1^2}\right) y^2 \\ -\overline{u'v'} &= -\,\overline{a_1 b_2}\; y^3 \end{aligned}\right\} \tag{10}$$

Equation (10) indicate that the growth rates of the turbulent kinetic energy and the Reynolds stress are proportional to the second and the third power of the distance from the wall, respectively.

In the Boussinesq eddy viscosity assumption, the Reynolds stress is given as;

$$-\overline{u'v'} = \nu_t \frac{\partial u}{\partial y} \tag{11}$$

Solving equations (5) and (11) for f_μ yields

$$f_\mu = \frac{-\overline{u'v'}}{C_{\mu f}\,(k^2/\varepsilon_p)(\partial u/\partial y)} \tag{12}$$

Consider $\varepsilon_p = 2\nu k_p/y^2 \approx$ constant and $u^+ \approx y^+$ for $y \sim 0$, where $u^+ = u/u_\tau$. Hence,

$$f_\mu \approx \frac{1}{y} \rightarrow \infty \quad \text{for} \quad y \rightarrow 0 \tag{13}$$

Inside the viscous sublayer ($0<y^+<5$), the molecular viscosity dominates over the turbulent viscosity; and in the fully turbulent region ($y^+>30\sim40$), the turbulent viscosity dominates over the molecular viscosity. Therefore, the wall damping function needs to satisfy the following constraints to correctly describe the physically observed near-wall turbulence field, that is

$$\left.\begin{aligned} f_\mu &\ll 1 \quad \text{for} \quad y^+ \approx 5 \\ f_\mu &\rightarrow 1 \quad \text{for} \quad y^+ \rightarrow 100 \end{aligned}\right\} \tag{14}$$

The wall damping function in the LMS is given as

$$f_\mu = \frac{1 - \exp\left(-\beta_1\sqrt{R_y} - \beta_2 R_y - \beta_3 R_y^2\right)}{1 - \exp\left(-\beta_4 R_y\right)} \tag{15}$$

and is shown in figure 2. The Taylor series expansion of equation (15) for y~0 clearly shows that $f_\mu \approx \beta_1/(\beta_4\sqrt{R_y}) \approx 1/y$ for R_y~0. The coefficients $\beta_i(i=1,4) = \{0.005, 0.001, 0.00011, 0.14\}$ are obtained by optimizing the constants to yield the best numerical results for the fully developed channel flow at $Re(u_\tau) = 180$.

For y~0, all the terms except the one containing the ε_p in equation (2) vanish. For the partial differential equation to be well posed at y~0, $f_{\varepsilon p}$ should vanish at y~0. Thus the wall damping function for the ε_p-equation is given as;

$$f_{\varepsilon p} = 1 - \alpha_{\varepsilon p}\exp\left(-R_y\right) \tag{16}$$

where $\alpha_{\varepsilon p} = 1.0$. For the ε_t-equation, equation (4), all the terms except the load functions become negligible at y~0. Thus equation (4) becomes an algebraic equation governing the ratio of $\varepsilon_t/\varepsilon_p$ at y~0. Since the production rate vanishes on the wall, the ratio of $\varepsilon_t/\varepsilon_p$ needs to be slightly greater than unity at the wall for the dissipation rate equation to be consistent with the inequilibrium analysis described in the following sub-section. Thus the wall damping function is given as

$$f_{\varepsilon t} = 1 - \alpha_{\varepsilon t}\exp\left(-R_y\right) \tag{17}$$

where $\alpha_{\varepsilon t} = 0.13$. The use of R_y in the wall damping functions (f_μ, $f_{\varepsilon p}$ and $f_{\varepsilon t}$) makes the influence of the wall proximity to disappear as the fully turbulent external region is approached and hence it renders the turbulence equations to be consistent with a physical observation that the turbulence length scale in the near-wall region is related to the normal

distance from the wall while that of the external flows is related to the flow field characteristics (Roshko 1976).

2.4. *Inherent capability of LMS equations*

The spectral density curves that correspond to different levels of P_r/ε_t and a partition representing the simplified split-spectrum are shown in figure 3(a). The spectral density curves are constructed based on the measured data of Klebanoff (1955) and Wygnanski & Fiedler (1969). The spectral density curves show that the energy-containing large eddies generated by the instability of the mean fluid motion are characterized by low frequency and the fine scale eddies in the dissipation range are characterized by high frequency. The curves also show that the ratio of k_p/k_t is determined by the shape and the frequency domain of each spectral density curve and that the ratio of k_p/k_t is large for large eddies and is small for fine scale eddies. Thus the cascade of turbulent kinetic energy is characterized by the ratio of k_p/k_t. The capability of the multiple-time-scale turbulence equations to model the cascade process is achieved by solving the splitted turbulent kinetic energy equations (k_p- and k_t-equation).

The inequilibrium analysis is based on the turbulence statics observed in the uniformly sheared flows (Tavoularis & Karnik 1989) and on the semi-empirical data used in the generalized algebraic stress turbulence models (Rodi 1972; Launder 1982; Kim & Chen 1988). For uniformly sheared flows and free-stream flows, the diffusion terms vanish. In such cases, dividing equation (1) by equation (3) yields (Kim & Benson 1992)

$$\frac{k_p}{k_t} = \frac{Dk_p/Dt}{Dk_t/Dt} = \frac{P_r/\varepsilon_t - \varepsilon_p/\varepsilon_t}{\varepsilon_p/\varepsilon_t - 1} \tag{18}$$

The existence of asymptotic states in which P_r/ε_t takes constant values that depend on the mean flow strain rates can be found in Tavoularis & Karnik (1989), and the dependence of $\varepsilon_p/\varepsilon_t$ on the ratio of P_r/ε_t can be observed in the semi-empirical data used in the generalized algebraic stress turbulence models as shown in figure 3(b). The eddy viscosity equation, equation (5), can be written in a form comparable with those of the generalized algebraic stress turbulence models and is given as

$$\mu_t = \rho c_\mu f_\mu \frac{k^2}{\varepsilon_t} \tag{19}$$

where $c_\mu = c_{\mu f}(\varepsilon_t/\varepsilon_p)$. Thus, in the multiple-time-scale turbulence model, the dependence of the eddy viscosity coefficient (c_μ) on the inequilibrium turbulence (P_r/ε_t) is described by the ratio of $\varepsilon_t/\varepsilon_p$. The turbulence model constants (c_{pi} and c_{ti}) obtained by solving an under-determined system of equations that governs the growth rate of the turbulence intensity in the uniformly sheared flows and the decay rate of the grid turbulence produce a c_μ-curve shown in figure 3(b). The under-determined model constants, subjected to constraint conditions obtained from a near-wall equilibrium analysis ($P_r=\varepsilon_p=\varepsilon_t$), are numerically optimized to yield best numerical results for simple shear layers such as a plane jet in a uniform stream and fully developed channel and pipe flows (Kim & Chen 1989; Kim 1991). It can be seen in figure 3(b) that $\varepsilon_t/\varepsilon_p<1$ and the ratio of P_r/ε_t increases faster than $\varepsilon_p/\varepsilon_t$ (i.e., the slope of $\left|(\varepsilon_t/\varepsilon_p)/(P_r/\varepsilon_t)\right|$ is less than unity) for the production dominated case ($P_r/\varepsilon_t>1$). In this case, $P_r>\varepsilon_p>\varepsilon_t$ so that equation (18) always yields a positive ratio of k_p/k_t, and the ratio of k_p/k_t is further increased as P_r/ε_t is increased. For turbulent flows in equilibrium state ($P_r=\varepsilon_p=\varepsilon_t$), equation (18) becomes indeterminate, and the ratio of k_p/k_t for

$P_r \approx \varepsilon_p \approx \varepsilon_t$ is determined by the imbedded constraint conditions. As the production rate becomes negligible ($P_r \approx 0$), $P_r < \varepsilon_t$ and the ratio of $\varepsilon_p/\varepsilon_t$ decreases faster than P_r/ε_t. In the latter case, $P_r < \varepsilon_p < \varepsilon_t$ so that equation (18) always yields a positive ratio of k_p/k_t, and the ratio of k_p/k_t is further decreased as P_r/ε_t is decreased. Therefore the trend of k_p/k_t distribution obtained in the inequilibrium analysis is in correct agreement with that observed in the spectral density curves shown in figure 3(a).

3. Computational results

3.1. *Fully developed channel flows*

Fully developed channel flows at $Re(u_\tau)$ = 180 and 395 are considered below. In each case, the flow domain in x-coordinate direction extends 70 channel heights in the downstream direction and that in the y-coordinate direction extends from the wall to the symmetric half of the flow domain. The computational domain is discretized by 97x91 grid points in x- and in y-coordinate directions, respectively. The grid size in the x-ccordinate direction is almost uniform while that in the y-coordinate direction is stretched by a factor of approximately 1.1. The smallest mesh size in the near-wall region is $\Delta y^+ \approx 0.25$. The inlet boundary condition is obtained by appropriately scaling measured data for a fully developed channel flow so that the calculated flow field may reach a fully developed state at a shorter downstream location from the inlet boundary. The numerical results presented herein are obtained at 5.5 channel heights upstream of the exit boundary so that the numerical results are not obscured by the exit boundary condition either. Examination of numerical results obtained using a few different mesh densities and extents of the flow domain shows that the numerical results presented herein are grid independent.

The numerical results for the normalized mean velocity ($u^+=u/u_\tau$), the turbulent kinetic energy ($k^+=k/u_\tau^2$), the Reynolds stress ($-\overline{u'v'}^+ = -\overline{u'v'}/u_\tau^2$) and the dissipation rate ($\varepsilon_t{}^+=\nu\varepsilon_t/u_\tau^4$) for $Re(u_\tau)=180$ are compared with the DNS results and the numerical results obtained using a RSM (Lai & So 1990) in figure 4. It can be seen in figure 4(a) that the calculated mean velocity profile is in excellent agreement with that obtained from the DNS. The growth rate and the peak value of the turbulent kinetic energy in the near-wall region obtained using the LMS is in better agreement with the DNS result than those obtained using the RSM as shown in figure 4(b). The calculated Reynolds stresses in figure 4(c) also show that the LMS yields improved numerical result than the RSM. The calculated dissipation rate is shown in figure 4(d). The slope of the dissipation rate obtained using the LMS is less steeper than that obtained from the DNS. The less steeper slope is caused by neglecting the turbulent diffusion term in deriving equation (7) and by the nonlinearity of the turbulence equations. The most distinguished difference between the LMS and the RSM as well as many other turbulence models can be observed in the calculated near-wall dissipation rates as shown in the figure. Extending the capability of the multiple-time-scale turbulence model to resolve the inequilibrium turbulence inside the near-wall layer enables the turbulence equations to yield a near-wall dissipation rate that is in qualitatively correct agreement with the DNS result.

Detailed comparisons of the various terms in the budget of the turbulent kinetic energy are shown in figure 5, where $\varepsilon_p{}^+ = \nu\varepsilon_p/u_\tau^4$ is the normalized energy transfer rate. It can be seen in the figure that each component obtained using the LMS overlaps with that obtained from the DNS in most part of the flow domain. The excellent comparisons between the LMS and

the DNS results indicate that the LMS can accurately resolve details of the near-wall turbulence structure. It can also be found in Lai & So (1990) that the present numerical results are in much better agreement with the DNS results than those obtained using the RSM, and the excellent agreement is attributed to the calculated near-wall dissipation rate that is in qualitatively correct agreement with the DNS result. The terms in the budget of k_p- and k_t-equation are shown in figures 5(b) and (c), respectively. It can be seen in the figures that the dissipation rate in the region very close to the wall is mostly balanced by the laminar viscous diffusion of the turbulent kinetic energy. The laminar viscous diffusion of the turbulent kinetic energy do not require any modelling and, hence, obtaining the correct dissipation rate at the wall depends on obtaining the correct near-wall distribution of the turbulent kinetic energy. Thus the qualitatively different near-wall dissipation rate obtained using the RSM is caused by the near-wall turbulent kinetic energy distribution that do not compare very well with the DNS result as shown in figure 4(b). Note that the near-wall energy transfer rate (ε_p) shown in figure 5(b) exhibits similar distribution as the dissipation rate obtained using single-time-scale turbulence models in the sense that the peak value is not located at the wall. Thus the dissipation rate that attains its peak value at the wall is caused by a small amount of the laminar viscous diffusion of the dissipation range turbulent kinetic (k_t) at the wall as shown in figure 5(c).

The composition of the turbulent kinetic energy is shown in figure 6(a). Since the peak production rate occurs at $y^+ \approx 12$ and the balance of the turbulent kinetic energy budget in the region below $y^+ \approx 12$ is mostly achieved by the laminar viscous diffusion, the turbulent kinetic energy in the region is mostly contained in the production range. The ratio of k_p/k_t is

also shown in figure 6(a). The viscous sublayer region is entirely dominated by the viscous diffusion and, hence, the inequilibrium analysis developed based on the turbulence statistics of uniformly sheared flows do not apply exactly in the region. Away from the viscous sublayer, the ratio of k_p/k_t is decreased as P_r/ε_t is decreased and, thus, the distribution of k_p/k_t is in correct agreement with the inequilibrium analysis. The near-wall distribution of $\varepsilon_t/\varepsilon_p$ is shown in figure 6(b). It can be seen in the figure that $\varepsilon_t/\varepsilon_p>1$ at the wall where the production rate vanishes, $\varepsilon_t/\varepsilon_p<1$ near $y^+\approx12$ where the production rate attains its peak value and $P_r/\varepsilon_t>1$, and $\varepsilon_t/\varepsilon_p>1$ again in the region remote from the wall where $P_r/\varepsilon_t<1$. Thus the calculated $\varepsilon_t/\varepsilon_p$ is in correct agreement with the inequilibrium analysis.

The numerical results for the mean velocity, the turbulent kinetic energy, the Reynolds stress and the dissipation rate for $Re(u_\tau)=395$ are compared with the DNS results in figure 7. It can be seen in the figure that the calculated mean velocity profile, the turbulent kinetic energy and the Reynolds stress are in excellent agreement with those obtained from the DNS. Each term in the budget of the turbulent kinetic energy for $Re(u_\tau)=395$ case exhibits improved comparison with the DNS results than the $Re(u_\tau)=180$ case, and the improved comparison is caused by the turbulent kinetic energy and the near-wall dissipation rate profiles that are in closer agreement with the DNS results than the $Re(u_\tau)=180$ case. Measured data show that the growth rate and the peak value of the turbulent kinetic energy are increased as the Reynolds number is increased (Patel et al. 1985). The turbulent kinetic energy obtained from the DNS also show that the growth rate and the peak value of the turbulent kinetic energy for $Re(u_\tau)=395$ are larger than those for $Re(u_\tau)=180$. Since the near-wall dissipation rate depends mostly on the growth rate and the peak

value of the turbulent kinetic energy near the wall, the peak value of the dissipation rate at the wall for $Re(u_\tau)=395$ is substantially larger than that for $Re(u_\tau)=180$. It can be seen in figure 7(d) that the LMS correctly predicts the increased near-wall dissipation rate.

3.2. *Pulsating pipe flows*

Pulsating pipe flows at a wide range of dimensionless frequency ($\omega^+=0.0075\sim0.21$) are considered below. In each case, the flow domain in x-coordinate direction extends 70 pipe diameters in the downstream direction and that in the y-coordinate direction extends from the wall to the center of the pipe. The computational domain is discretized by 144x64 grid points in x- and in y-coordinate directions, respectively. The grid size in the x-ccordinate direction is almost uniform while that in the y-coordinate direction is stretched by a factor of approximately 1.1. The smallest mesh size in the near-wall region is approximately equal to 1/15 δ_s (which corresponds to $\Delta y^+\approx0.25\sim0.8$ for different Reynolds numbers), where $\delta s=\sqrt{2\nu/\omega}$ is the Stokes layer thickness, $\omega=2\pi f$ is the angular velocity, and f is the frequency. This mesh is fine enough to resolve the influence of the imposed frequency on the near-wall fluid flow and to yield a grid independent solution. The transient bulk velocity is prescribed as $u_b = \overline{u_b}\{1+|\widetilde{u_b}|\sin(\omega t)\}$, where $\overline{(\,)}$ denotes the time-averaged value, $\widetilde{(\,)}$ denotes the ensemble-averaged value, and $|\widetilde{(\,)}|$ denotes the amplitude. The boundary condition for the axial velocity that corresponds to the time-varying bulk velocity is obtained by scaling measured data for a fully developed pipe flow so that the calculated flow field may reach a fully developed state at a shorter downstream location from the inlet boundary. The numerical results presented herein are obtained at 4 diameters

upstream of the exit boundary so that the numerical results are not obscured by the exit boundary condition either. Numerical tests show that the calculated results become independent of the time-step size for $\Delta T<T/200$, where T is the period. The numerical results presented herein are are obtained using $\Delta T=T/300$.

The calculated time-averaged wall shearing stresses for Re=15000~60000 and the ensemble-averaged wall shearing stresses for a few representative cases are shown in figures 8 and 9, respectively. It can be seen in figure 8 that the calculated wall shearing stresses are in very good agreement with the measured data for the wide range of Reynolds number. The ensemble-averaged wall shearing stress for Re = 15400, $|\widetilde{u_b}|/u_b$ = 0.1, and f = 0.625 Hz is shown in figure 9(a). This pulsating flow represents an extreme case of a low Reynolds number flow subjected to a high frequency oscillation. In such a case, the spatial variation of the oscillating velocity is mostly confined in the near-wall region so that the amplitude of the wall shearing stress is a several times larger than that of the ensemble-averaged centerline velocity (Mao & Hanrathy 1986). It can be seen in the figure that the calculated phase difference is in good agreement with the measured data while the calculated amplitude is larger than the measured data. The over-predicted amplitude is caused by a slightly over-predicted turbulent viscosity in the core region of the pipe. The case shown in figure 9(c) represents an opposite extreme case of a high Reynolds number flow subjected to a low frequency oscillation. The Reynolds number is 60000, $|\widetilde{u_b}|/u_b$ = 0.05, and f=0.325 Hz. It can be seen in the figure that the calculated and the measured amplitudes are by far smaller than those shown in figure 9(a). The highly decreased amplitude is caused by the large Reynolds number and the small amplitude of the

ensemble-averaged centerline velocity. The calculated and the measured wall shearing stresses for an intermediate case of Re=15400, $|\widetilde{u_b}|/u_b$ = 0.05, and f = 0.625 Hz are shown in figure 9(b). In each case, the amplitude of the wall shearing stress is over-predicted while the calculated shape and phase lead of the ensemble-averaged wall shearing stress are in very good agreement with the measured data. It can be found in Kebede et al. (1985) that the shape, phase lead and the amplitude of the ensemble-averaged wall shearing stresses obtained using a k-ε turbulence model and a RSM do not compare favorably with the measured data. The significantly improved numerical results obtained using the LMS indicate that the turbulence equations can correctly describe the influence of the Reynolds number and the imposed oscillation frequency on the fluid flow.

The calculated phase lead of the wall shearing stress with respect to the ensemble-averaged centerline velocity is shown in figure (10), where $\phi=\omega t$ is the phase angle. It is shown in the figure that the calculated phase lead for $\omega^+>0.045$ (or $\omega^+/15>0.003$) obtained using the LMS is in better agreement with the measured data than that obtained using the RDT which is developed to accurately solve pulsating pipe flows at high dimensionless frequency. It can be found in Mao & Hanrathy (1986) that the present numerical result is in as good agreement with the measured data as that obtained using an optimized relaxation turbulence model. It can also be seen in the figure that the LMS correctly predicts the rapidly varying phase lead that occurs for $\omega^+<0.015$ (or $\omega^+/15<0.001$) while RDT and various other turbulence models fail to predict such a phenomenon (Mao & Hanrathy 1986; Mankbadi & Liu 1992).

The calculated ratio of the normalized amplitude of the wall shearing stress to that of the centerline velocity is shown in figure 11. It can be seen

in the figure that the present numerical result for high dimensionless frequency range is in as good agreement with the measured data as that obtained using the RDT. It can also be seen in the figure that the LMS yields qualitatively correct numerical result for $\omega^+<0.015$ (or $\omega^+/15<0.001$) while the RDT completely fail to predict the experimentally observed behavior of the pulsating pipe flow.

4. Conclusions and discussion

A low Reynolds number multiple-time-scale turbulence model that can resolve the inequilibrium turbulence phenomena down to the viscous sublayer is presented. The capability to resolve the inequilibrium turbulence phenomena inside viscous sublayer enables the LMS to yield a near-wall dissipation rate that is in correct agreement with the DNS result. It is shown that the near-wall turbulence structure for the low Reynolds number fully developed channel flows obtained using the LMS is in better agreement with the DNS results than those obtained using a Reynolds stress model. Each term in the budget of the turbulent kinetic energy obtained using the LMS is in excellent agreement with that obtained from the DNS, and the excellent agreement is caused by the near-wall dissipation rate that is in correct agreement with the DNS result.

Calculations of unsteady turbulent flows using algebraic turbulence models, k-ε turbulence models and Reynolds stress turbulence models show that the numerical results obtained using the algebraic turbulence models are in much better agreement with the measured data than those obtained using k-ε turbulence models or Reynolds stress turbulence models (Kebede et al. 1985; Mankbadi & Liu 1992; Mao & Hanrathy 1986). The improved numerical results obtained using the algebraic turbulence models

clearly indicate that the algebraic turbulence models can describe the transient near-wall turbulent viscosity more accurately than k-ε turbulence models or Reynolds stress turbulence models. However, optimized algebraic turbulence models can not resolve the turbulence field of various complex turbulent flows and lack a theoretical background (Mao & Hanrathy 1986). It is shown that the low Reynolds number multiple-time-scale turbulence model (LMS) yields highly improved numerical result for the pulsating pipe flows at a wide rage of the dimensionless frequency than the algebraic turbulence model derived from the rapid distortion theory (RDT). For pulsating pipe flows at high dimensionless frequency, the spatial variation of oscillating velocity is mostly confined in the near-wall region. Therefore, a turbulence model that yields only a slightly deteriorated numerical results for steady flows may yield a largely deteriorated numerical result for pulsating flows. It is shown in the fully developed channel flow calculations that the near-wall dissipation rate that attains its peak value at the wall yields improved near-wall turbulence structure than the near-wall dissipation rate that attains its peak value at $y^+ \approx 12$. The improved numerical results for the pulsating pipe flows obtained using the LMS is attributed to its capability to resolve the near-wall turbulence structure more accurately than other turbulence models.

Numerical investigations of various complex turbulent flows show that the multiple-time-scale turbulence model yields as accurate numerical results as those obtained using an optimized turbulence model for each flow (Kim & Chen 1989; Kim 1990, 1991; Kim & Benson 1992). These accurate numerical results indicate that the developments of the fluid flow and the turbulence field in complex turbulent flows depend strongly on the inequilibrium turbulence. The improved numerical results for the fully

developed channel flows and the pulsating pipe flows obtained using the LMS indicate that the development of the near-wall turbulence field also depends strongly on the inequilibrium turbulence. The capability of the multiple-time-scale turbulence model to resolve various complex turbulence fields is attributed to its capability to model the cascade of turbulent kinetic energy and to correctly resolve the inequilibrium turbulence phenomena.

Acknowledgement

This work is supported by NASA Grant #NCC3-229. Sincere thanks go to Dr. Reda Mankbadi for many helpful discussion.

REFERENCES

Hanjelic, K., Launder, B. E. & Schiestel, R. 1980 Multiple-time-scale concepts in turbulent shear flows. In *Turbulent shear flows* 2 (ed. Bradbury, L. J. S., Durst, F., Launder, B. E., Schmidt, F. W. & Whitelaw, J. H.), 36-49, Springer.

Kebede, W., Launder, B. E. & Younis, B. A. 1985 Large-amplitude periodic pipe flow: A second-moment closure study. *Fifth Symp. on Turbulent Shear Flows, Cornell University, Ithaca, New York* (ed. L. J. S. Bradbury, B. E. Launder, F. W. Schmidt, J. H. Whitelaw). Springer.

Kim, J., Moin, P. & Moser, R. 1987 Turbulence statistics in fully developed channel flow at low Reynolds number. *J. Fluid Mech.* **177**, 133-186.

Kim, S.-W. 1990 Numerical investigation of separated transonic turbulent Flows with a multiple-time-scale turbulence model. *Numerical Heat Transfer* Part A **18**, 149-171.

Kim, S.-W. 1991 Calculation of reattaching shear layers in divergent channel with a multiple-time-scale turbulence model. *AIAA J.* **29**, 547-554

Kim, S.-W. & Benson, T. J. 1991 Comparison of SMAC, PISO and iterative time-advancing schemes for self-sustained unsteady flows. *NASA TM-*104406.

Kim, S.-W. & Benson, T. J. 1992 Calculation of a circular jet in crossflow with a multiple-time-scale turbulence model. *Int. J. Heat Mass Transfer* To appear.

Kim, S.-W & Chen, C.-P. 1989 A multiple-time-scale turbulence model based on variable partitioning of the turbulent kinetic energy spectrum. *Numerical Heat Transfer* Part B **16**, 193-211

Kim, S.-W. & Chen, Y.-S. 1988 A finite element calculation of turbulent boundary layer flows with an algebraic stress turbulence model. *Computer Methods in Applied Mechanics and Engineering* **66**, 45-63.

Klebanoff, P. S. 1955 Characteristics of turbulence in a boundary layer with zero pressure gradient. *NACA* Report 1247

Lai, Y. G. & So, R. M. C. 1990 On near-wall turbulent flow modelling. *J. Fluid Mech.* **221**, 641-673.

Launder, B. E. 1982 A generalized algebraic stress transport hypothesis. *AIAA J.* **20**, 436-437.

Mankbadi, R. R. & Liu, J. T. 1992 Near-wall response in turbulent shear flows subjected to imposed unsteadiness. *J. Fluid Mech.* To appear.

Mao, Z.-X. & Hanrathy, T. J. 1986 Studies of the wall shear stress in a turbulent pulsating pipe flows. *J. Fluid Mech.* **170**, 545-564.

Patel, V. C., Rodi, W., & Scheuerer, G. 1985 Turbulence models for near-wall and low-Reynolds-number flows: A review. *AIAA J.* 23, 1308-1319.

Rodi, W. 1972 The prediction of free boundary layers by use of a two-equation model of turbulence. Ph.D. thesis, University of London, London.

Roshko, A. 1976 Structure of Turbulent Shear Flows: A New Look. *AIAA J.* **14**, 1349-1357.

Tavoularis, S. & Karnik, U. 1989 Further experiments on the evolution of turbulent stresses and scales in uniformly sheared turbulence. *J.Fluid Mech.* **204**, 457-478

Wygnanski, I. & Fiedler, H. 1969 Some measurements in the self-preserving jet. *J.Fluid Mech.* **3**, 577-612

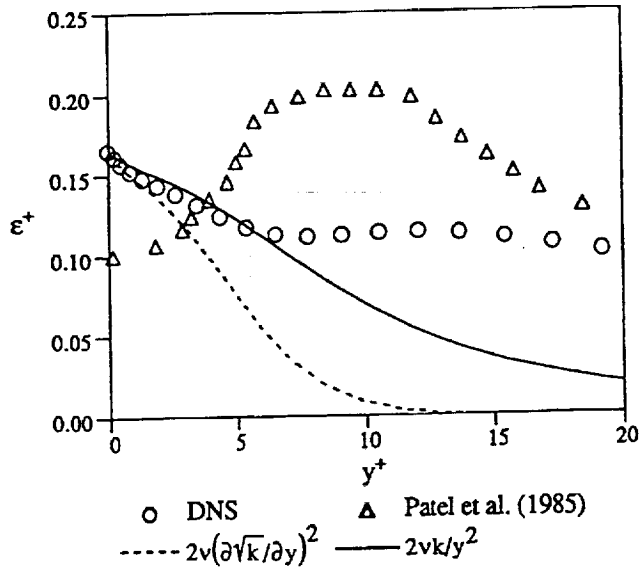

Figure 1.—ϵ_p and ϵ_t inside viscous sublayer.

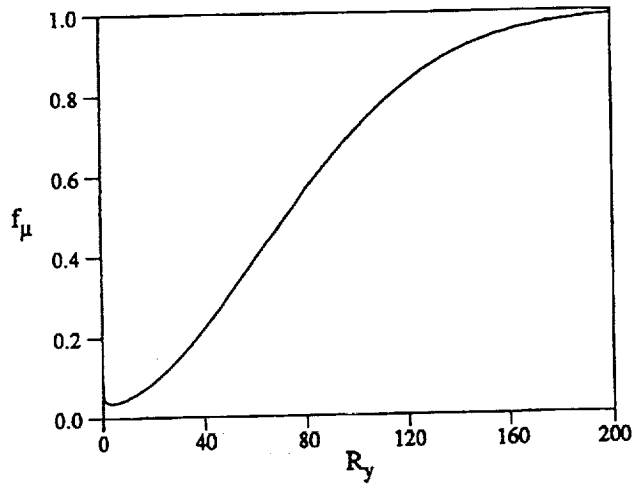

Figure 2.—Wall Damping function (fμ).

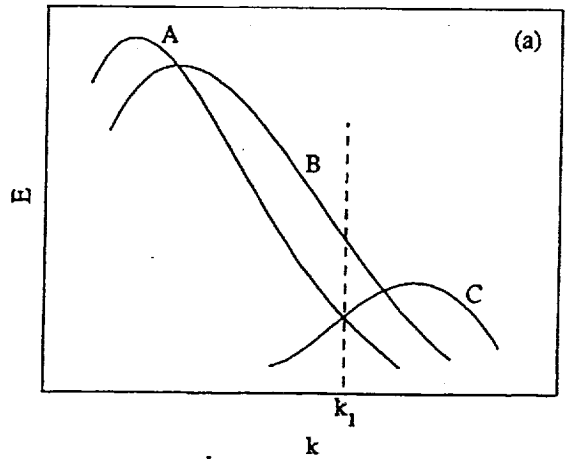

$$k_p = \int_0^{k_1} E\,dk, \qquad k_t = \int_{k_1}^{\infty} E\,dk$$

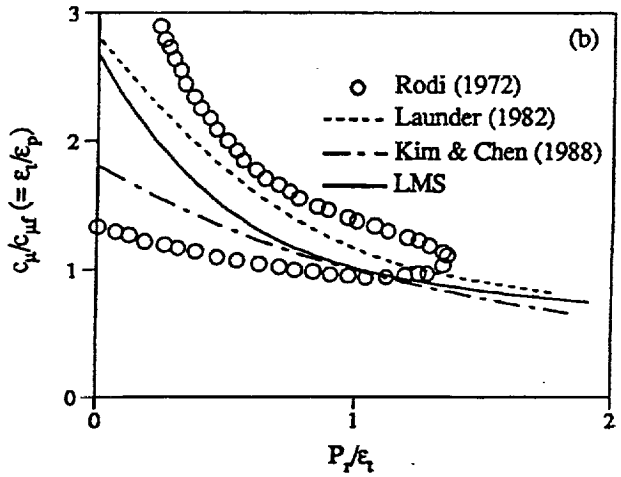

Figure 3.—Turbulent flows in inequilibrium state (Kim & Benson 1992).
(a) Spectral density curves, k: wave number, E: Energy spectral density, $(P_r/\epsilon_t)A > (P_r/\epsilon_t)B > (P_r/\epsilon_t)C$,
(b) Semi-emperical data for eddy viscosity coefficient.

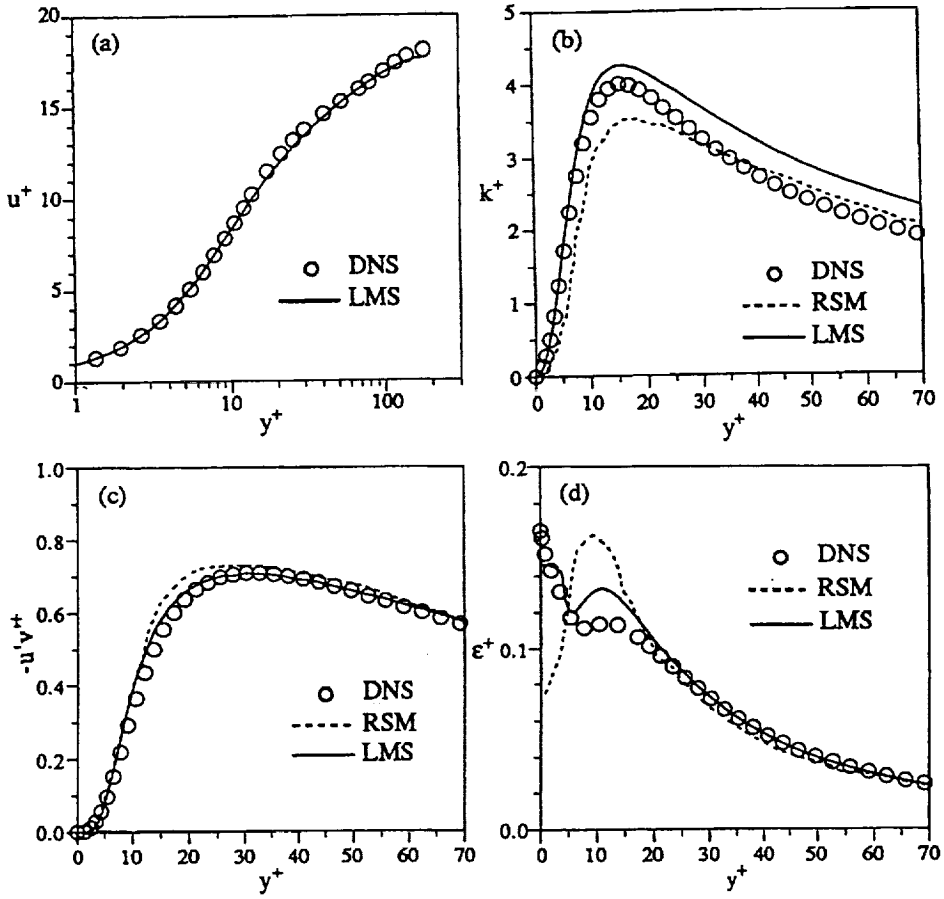

Figure 4.—Fully developed channel flow at $Re(u_\tau) = 180$.
(a) Mean-velocity profile.
(b) Turbulent kinetic energy profile.
(c) Reynolds Stress.
(d) Dissipation rate.

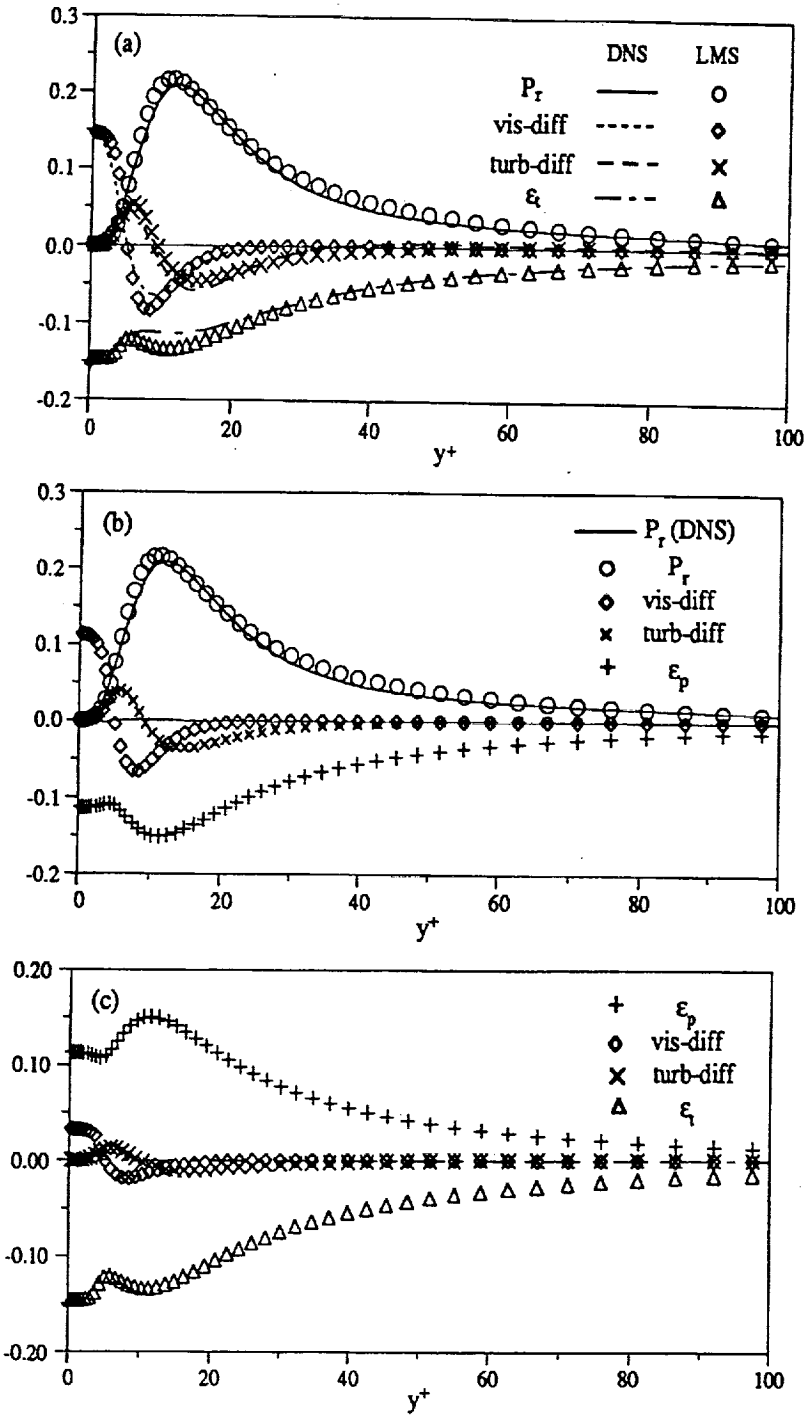

Figure 5.—Budget of turbulent kinetic energy.
(a) Total turbulent kinetic energy ($k = k_p + k_t$).
(b) k_p in the production range.
(c) k_t in the dissipation range.

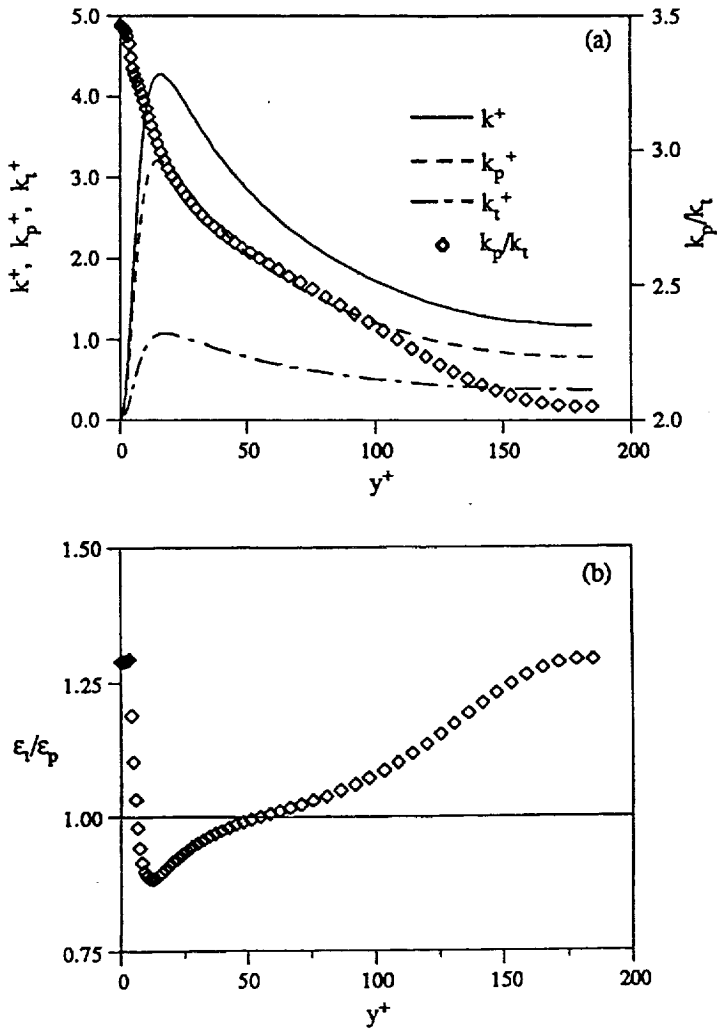

Figure 6.—Inequilibrium turbulence structure inside shear layer.
(a) Turbulent kinetic energy.
(b) ϵ_t/ϵ_p.

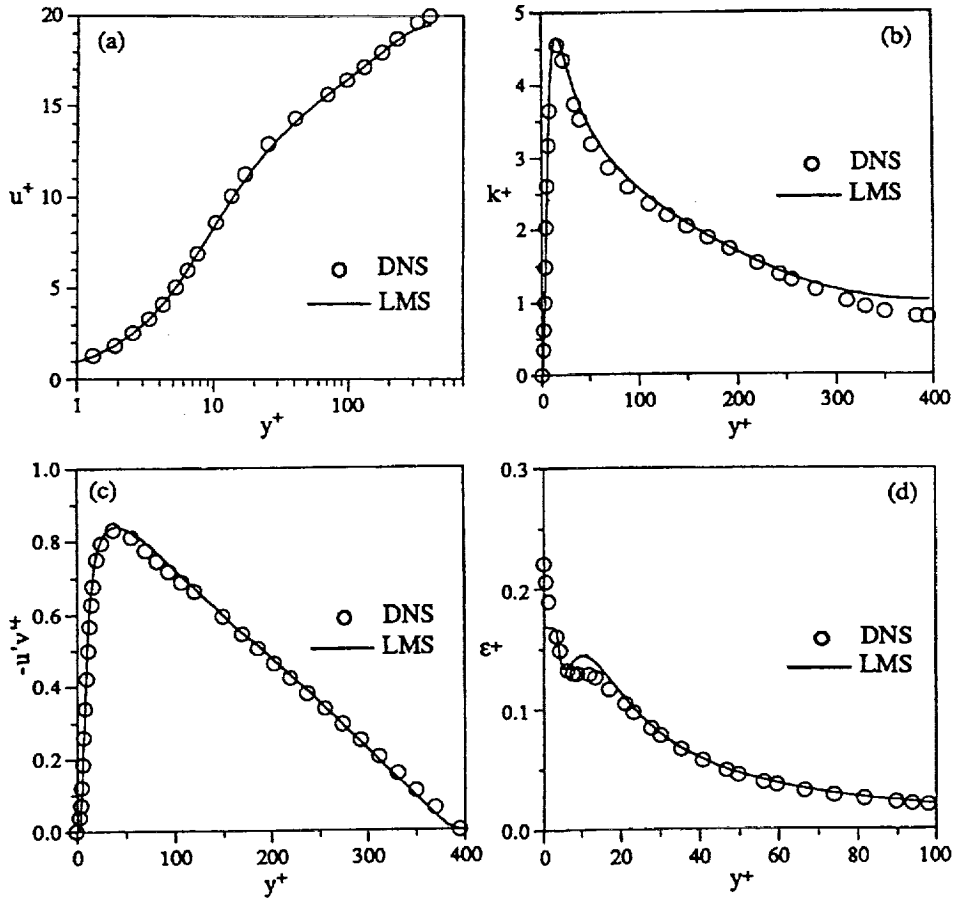

Figure 7.—Fully developed channel flow at Re(u_τ) = 395.
(a) Mean-velocity profile.
(b) Turbulent kinetic energy profile.
(c) Reynolds stress.
(d) Dissipation rate.

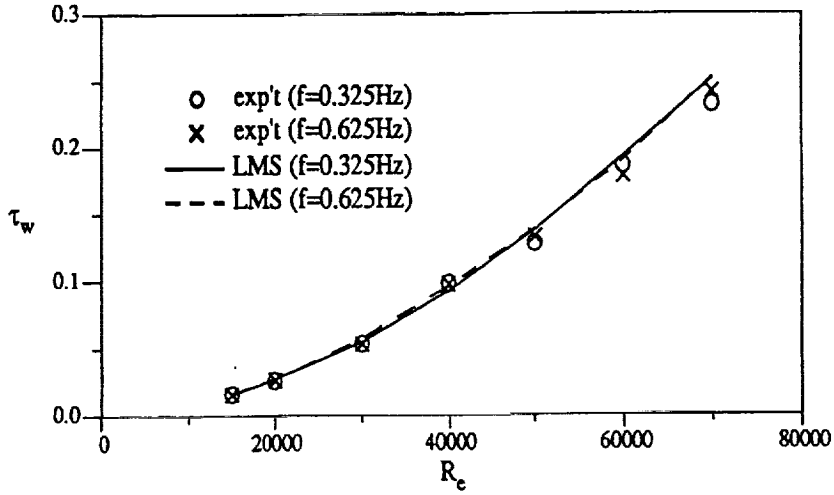

Figure 8.—Time-averaged wall shearing stress for pulsating pipe flow.

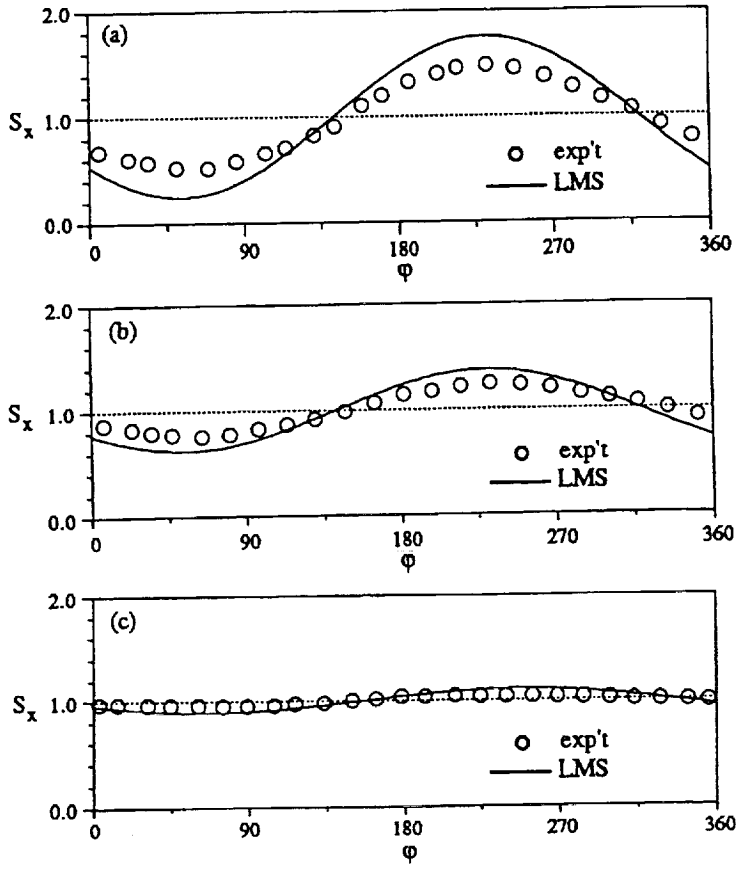

Figure 9.—Ensemble-averaged velocity gradient at the wall for pulsating pipe flows.
(a) Re = 15400, f = 0.625 Hz, $|\tilde{u}_b|/\overline{u}_b = 0.1$.
(b) Re = 15400, f = 0.625 Hz, $|\tilde{u}_b|/\overline{u}_b = 0.05$.
(c) Re = 60000, f = 0.325 Hz, $|\tilde{u}_b|/\overline{u}_b = 0.05$.

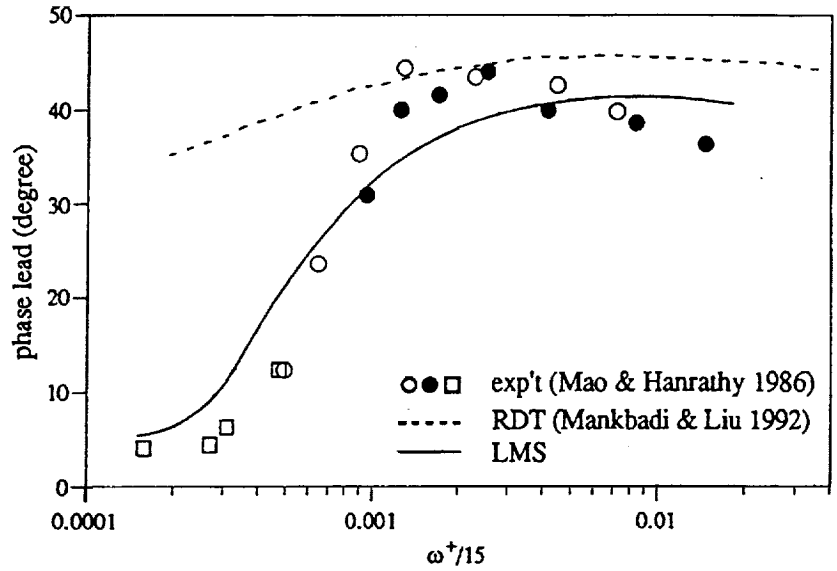

Figure 10.—Phase lead of velocity gradient at the wall.

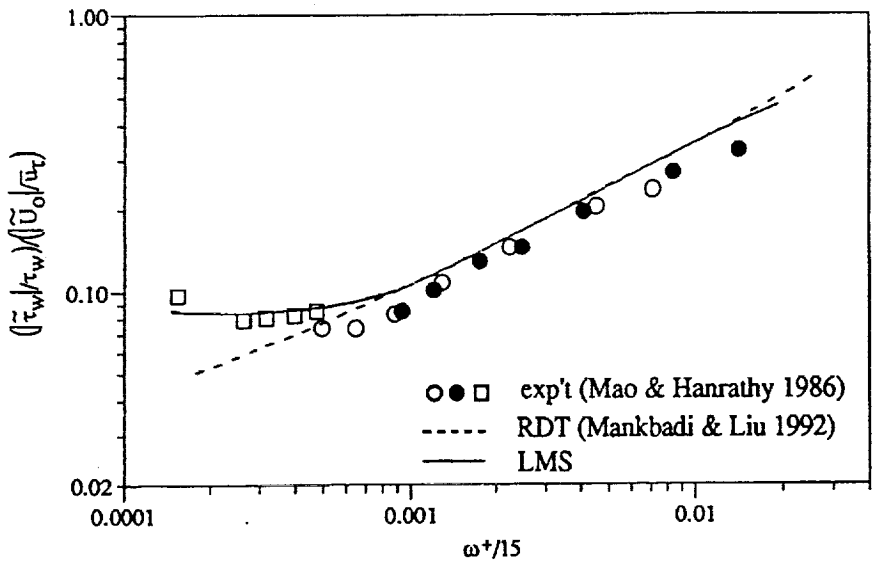

Figure 11.—Ratio of amplitude of velocity gradient at the wall to amplitude of centerline velocity.

REPORT DOCUMENTATION PAGE

Form Approved
OMB No. 0704-0188

1. AGENCY USE ONLY (Leave blank)	2. REPORT DATE	3. REPORT TYPE AND DATES COVERED
	May 1992	Final Contractor Report

4. TITLE AND SUBTITLE

Low Re Multiple-Time-Scale Turbulence Model and Calculations of Steady and Pulsating Shear Layers

5. FUNDING NUMBERS

WU–505–62–52
C–NCC3–229

6. AUTHOR(S)

Sang-Wook Kim

7. PERFORMING ORGANIZATION NAME(S) AND ADDRESS(ES)

University of Toledo
Toledo, Ohio 43606

8. PERFORMING ORGANIZATION REPORT NUMBER

E–7038

9. SPONSORING/MONITORING AGENCY NAMES(S) AND ADDRESS(ES)

National Aeronautics and Space Administration
Lewis Research Center
Cleveland, Ohio 44135–3191

10. SPONSORING/MONITORING AGENCY REPORT NUMBER

NASA CR–189176

11. SUPPLEMENTARY NOTES

Project Manager, Robert M. Stubbs, Internal Fluid Mechanics Division, NASA Lewis Research Center, (216) 433–6303.
Sang-Wook Kim, University of Toledo and NASA Resident Research Associate at Lewis Research Center.

12a. DISTRIBUTION/AVAILABILITY STATEMENT

Unclassified - Unlimited
Subject Category 34

12b. DISTRIBUTION CODE

13. ABSTRACT *(Maximum 200 words)*

A low Reynolds number multiple-time-scale turbulence model (LMS) and its application to fully developed turbulent channel flows and pulsating pipe flows are presented. The LMS can describe the inequilibrium turbulence phenomena down to the viscous sublayer. The calculated fluid flow and turbulence fields for the channel flows are in better agreement with the direct numerical simulation (DNS) results than those obtained using a Reynolds stress turbulence model, and the calculated near-wall dissipation rates are in qualitatively correct agreement with DNS results. The LMS also successfully predicts the rapidly varying phase-lead of the wall shearing stress that occurs in a narrow range of the dimensionless frequency ($\omega^+ = \omega\nu/u_\tau^2$) for the pulsating pipe flows while various other turbulence models fail to predict this phenomenon, and the LMS yields significantly improved numerical results for a wide range of the dimensionless frequency compared with those obtained using a rapid distortion theory (RDT).

14. SUBJECT TERMS

Unsteady flow; Turbulence; Computational fluid dynamics

15. NUMBER OF PAGES

36

16. PRICE CODE

A03

17. SECURITY CLASSIFICATION OF REPORT	18. SECURITY CLASSIFICATION OF THIS PAGE	19. SECURITY CLASSIFICATION OF ABSTRACT	20. LIMITATION OF ABSTRACT
Unclassified	Unclassified	Unclassified	